http://eprints.gla.ac.uk/228031/

Wireless Communication and Power Harvesting in Wearable Contact Lens Sensors

Mengyao Yuan, *Student Member, IEEE*, Rupam Das, *Member, IEEE*, Eve McGlynn,
Student Member, IEEE, Rami Ghannam, *Senior Member, IEEE,* Qammer H. Abbasi,
Senior Member, IEEE and Hadi Heidari, *Senior Member, IEEE*

Abstract—The human eye contains multiple biomarkers related to various diseases, making electronic contact lens an ideal non-invasive platform for their diagnosis and treatment. Recent advances in technology have enabled the monitoring and diagnosis of glaucoma from Intraocular Pressure (IOP) detection, diabetes from glucose concentration detections, and other biosensors for pH and temperature sensing. Different sensor designs have led to distinct power transfer techniques, among which inductively coupled power transfer is considered most favourable for electronic contact lenses power delivery applications. Therefore, loop antenna, spiral shape antenna, and antenna with nanomaterials such as graphene and hybrid silver nanofibers have been explored under Industrial, Scientific, and Medical (ISM) frequency bands for both Wireless Power Transfer (WPT) and data communication. Notably, spiral antennas are also considered as the component of IOP sensing using capacitive sensors to detect the changes in frequency caused by pressure. This article reviews the state-of-the-art technologies in electronic contact lens sensors and their power delivery techniques. Herein, diverse sensing methods, materials, and power transfer techniques and the promising future trends and challenges in electronic contact lenses have been presented.

Index Terms—Electronic contact lens, wireless power transfer, sensors, energy harvesting, wearable electronics.
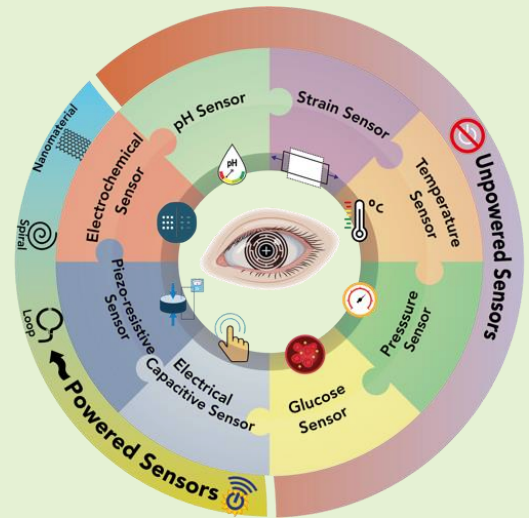
I. Introduction

ELECTRONIC wearable devices have been widely recognized as the next hot topic in the field of the smart terminal industry [1], particularly since the innovation space of smartphones is narrowing and their market growth approaches saturation [2-4]. Most wearable devices possess particular data processing functions, which are connected with mobile phones and portable accessories. Widespread studied cases include those supported by the wrist [5-12], shoes [12, 13], skin [14-16], e-textiles [17-20], glasses [21-23] and other types of non-mainstream products [24, 25]. To ensure maximum wearer comfort, wearable devices need to be both lightweight and small [26]. Technologically developed and commercialized wearable sensors aim to monitor human health through vital signs associated with healthcare, sports, or medical applications [27-29], where the majority of subsistent wearable devices focus mainly on the assessment of physical parameters (*e.g.* motion, respiration rate) or electrophysiology (*e.g.* Electrocardiogram, Electromyography). Unlike conventional

wearable devices, electronic contact lenses can make use of both physical and chemical sensors for a variety of applications. For example, physical sensors can detect glaucoma via pressure sensing [30-32], whereas chemical sensors can detect Diabetes by sensing changes in glucose concentration. Additionally, continuous measurements are of vital importance that in the cases of diabetes and glaucoma, the effects of continuous monitoring have been observed and modelled, indicating that improved management of these conditions significantly reduces the need for hospital treatment. Continuous blood sugar monitoring reduces the risk of diabetic ketoacidosis by a factor of four [33]; continuous pressure monitoring decreases the financial burden of glaucoma by 20% [34]. In the future, electronic contact lenses can also integrate sensing and drug delivery. Fig. 1 summarises the historical development of electronic contact lens design, as well as future perspectives.

The search for an alternative to blood samples for non-invasive disease diagnosis has been explored for decades in which cerebrospinal fluid, urine, saliva, and tears are considered suitable substitutes where they have unique advantages in diagnosing specific diseases [35-38]. The analyte concentrations in tears and biomedical component characteristics for human eyes are confined within normal ranges [39-47] in healthy individuals. When the analyte concentration is beyond the specific range (Table I), this leads to related diseases [48-52]. Therefore, multiple biomarkers in tear fluids may be used for disease screening.
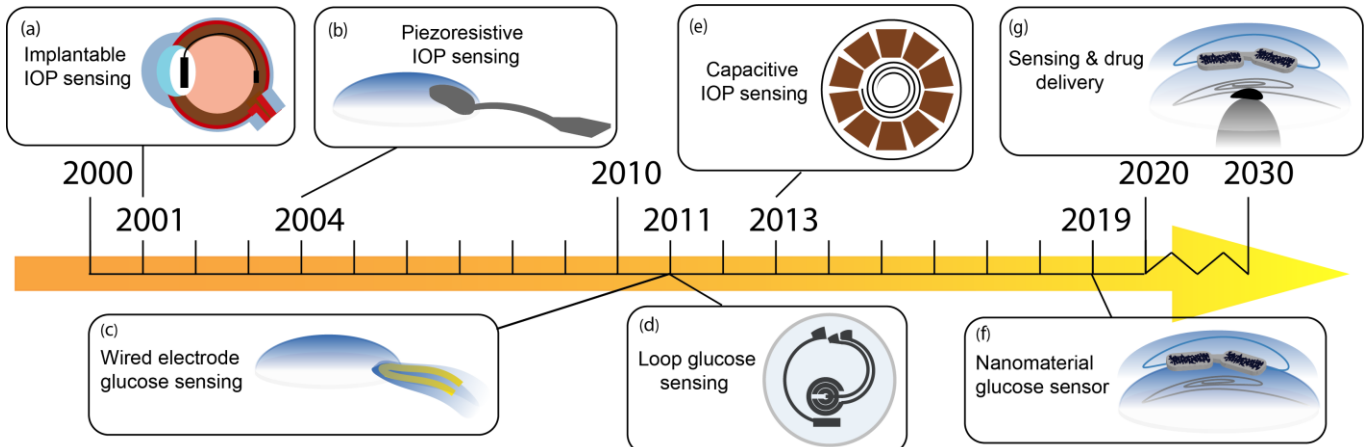
Fig. 1. Electronic Contact Lenses design history: (a) Implantable IOP sensing during 2000s [59], (b) First piezo-resistive IOP sensing was explored in 2004 for wearable glaucoma detection [97], (c) Wired glucose sensing for diabetes diagnose in 2010s [66], (d) Loop glucose design for wireless preparation in 2011 [70], (e) Capacitive IOP sensing utilizing frequency shifts due to impedance change by applied pressure [131], (f) Combination of nanomaterials, glucose and IOP sensing in 2019 [145], (g) Disease diagnosing and drug delivery integrated in the future.

In general, the tear fluid film is mainly composed of three layers: Mucin, Aqueous, and Lipid [53, 54], which play the role of lubrication and cleaning. It is interesting to note that the components of tears are similar to blood since plasma penetrates the blood-tear barrier [55]. Thus, the advantage of an electronic contact lens is that it is a non-invasive approach to disease diagnosing through integrated biosensors. Although most aspects of the two body fluids are different, plasma leakage can be detected in tears instead of blood. As a result, an electronic contact lens presents a platform for disease diagnoses and treatments through direct contact with the eyeball and tears fluids, where the analyte concentrations in tear fluids are similar to those in blood for chemical sensing [40, 56, 57]. In addition to its direct contact with body fluid, this miniaturized integrated electronic contact lens needs to be transparent to maintain natural vision. Furthermore, the contact lens should be encapsulated with biocompatible materials, where the union between micron-scale integration techniques and materials becomes a significant challenge [58].

Advanced contact lens sensors vary from pH, temperature, pressure, and chemical sensing applications, where their powering methods also change simultaneously. The application varies from first implantable sensing [59] to future simultaneous wireless sensing and drug deliveries. Contact lens sensors fabricated with photonic crystals, liquid crystals and phenylboronic acid react directly with pressure, temperature, and glucose molecules, which means they do not require an external power transfer unit [60-64]. Nevertheless, glaucoma or glucose detection using electrical and electrochemical sensors require power generation by either wired or wireless power transfer [65-70].

We, therefore, provide a systematic review that demonstrates how WPT has been successfully used in facilitating power transfer to electronic contact lenses. Using standardized steps of conducting a systematic review, an initial set of 73 articles were identified, with almost a quarter of these appearing within the past 2-years. Among them, 13 papers addressed unpowered sensors, which studied contact lenses under various biomedical scenarios such as photonic and liquid crystals used for pressure and temperature sensing. Electrical and electrochemical sensors are covered in 29 publications, which mainly report the sensing principles, power consumptions, applied materials, and unique power transferring technologies. The final 31 key publications compare different WPT technologies used in electronic contact lenses and include the latest advances of contact lens antenna combined with nanomaterials. This review presents an overview of the latest trends, as well as recommendations for future directions. We also provide a summary of emerging technologies, where advances in nanomaterials will be critically crucial for electronic contact lenses development.

II. CONTACT LENS SENSORS

A. Unpowered Sensors

Unpowered sensors have recently attracted attention in wearable electronic devices for their inherent advantages of flexibility and comfortability, especially when interfacing with wearable layers in contact with the skin without any electrical components [71-74]. Unpowered biosensors on electronic contact lenses are widely used for pressure, strain, glucose, pH, and temperature sensing. In such cases, smartphones and optical microscopes are generally used for data processing, those unpowered sensors rely on external devices to transfer

TABLE I
ANALYTE CONCENTRATIONS AND COMPONENT RANGES IN TEARS

Analyte/Component	Normal Range	Related Disease	Ref
K^+	$20 - 42\ mM$	Hyperkalaemia	[39, 40]
Ca^+	$0.4 - 1.1\ mM$	Lacrimal cystic fibrosis	[39, 40, 49]
Na^+	$120 - 165\ mM$	Lacrimal cystic fibrosis	[40,41,49]
Cl^-	$118 - 135\ mM$	Dry eye disease	[39, 40, 41]
pH	6.4-7.7	Dry eye disease	[43, 83]
HCO_3^-	$20 - 42\ mM$	Dry eye disease	[39, 40, 41]
Zn^+	$23.2 - 52.5$ ng/ml	Keratitis	[44, 50]
Cu^+	$4.60 - 9.75$ ng/ml	Hepatopathies	[44, 52]
Lactoferrin	$1.01 - 3.43$ mg/ml	Keratoconjunctivitis	[45, 51]
Lactate	$2 - 5\ mM$	Lactic acidosis	[39, 40]
Glucose	$0.1 - 0.6\ mM$	Diabetes	[40]
Protein	$5 - 11\ mM$	Inflammation	[46, 55]
IOP	$10 - 20\ mmHg$	Glaucoma	[47]

2

information either through light, colour, or microfluidic detections.

Typically, microfluidic strain sensing depends on the resistivity change caused by mechanical deformations. However, Agaoglu *et al.* presented microfluidic dilatometric sensing for an electronic contact lens (Fig. 2(a)) based on the total volume change detection [60]. That strain sensor was composed of a liquid reservoir, an air reservoir, and a liquid-air interface on the sensing channel for strain detection. A five-ring structure was fabricated with Norland Adhesive (NOA) 65 [61] oil to increase the sensitivity up to 15.5 mm liquid channel change per 1% applied horizontal strain under 40 mmHg pressure range. Additionally, the microfluidic NOA65 sensor also presented the potential of temperature sensing since it had similar physical principles as commercialized thermometers. However, for those transparent NOA materials and Polydimethylsiloxane (PDMS) encapsulation, it is hard to detect and read the exact liquid movement position. In contrast, An *et al.* designed a microfluidic IOP sensor with dyed red liquid (Fig. 2(b)) to make a more precise illustration of the pressure output [62]. That microfluidic sensor contained a dyed liquid-filled sensing chamber, liquid flow sensing channels, and a buffer chamber to avoid liquid leakage. When different intraocular pressures were applied on the contact lens surface, dyed liquid flows from the sensing chamber to the sensing channels and the displacement can be read relative to the pressure value. With that sensor design, the sensitivity can reach 0.2832 mm/mmHg under a pressure range of 0 mmHg to 40 mmHg. However, the accurate pressure value has to be processed using an external optical microscope, which limits the sensing conditions and significantly reduces real-time practicability.

Other than microfluidic IOP sensing, photonic crystal-based sensors present a quantifiable platform of measurement due to its accurate RGB values. As shown in Fig. 2(c), where the IOP sensor was fabricated with a photonic crystal on top of a circular micro hydraulic amplifier system, the applied pressure was enlarged by the micro hydraulic system [63]. According to Bragg's equation [75-77],

$$m\lambda = 2dn_{eff}sin\theta \qquad (1)$$

where m is the order of diffraction, d is the spacing between the planes in the lattice, n_{eff} is the mean refractive index of the system, and θ is the glancing angle between the incident light and diffraction crystal planes. The lattice distance change in the photonic crystal results in a wavelength shift, which can then be captured by an optical microscope or mobile phone camera, where the sensitivity can reach 0.23 nm per mmHg with a testing range up to 110 mmHg.

The same Bragg reflection theory can also be applied to temperature sensing. A contact lens with temperature sensors on four active temperature positions [78] was fabricated by Moreddu *et al.*, where the sensors were made of thermochromic liquid crystal (TLC) due to its rapid and accurate temperature sensing (Fig. 2(d)) on wearable devices [79-81]. Four temperature mapping positions were used, which were Central, Peripheral, Limbal, and Paracentral. These positions were etched with TLC sensors and the wavelength of each TLC sensor shifts when the heating is applied. The experimental temperature range was 29°C to 40°C, at increments of 0.5°C. Besides, the light scattering phenomenon is also applicable for
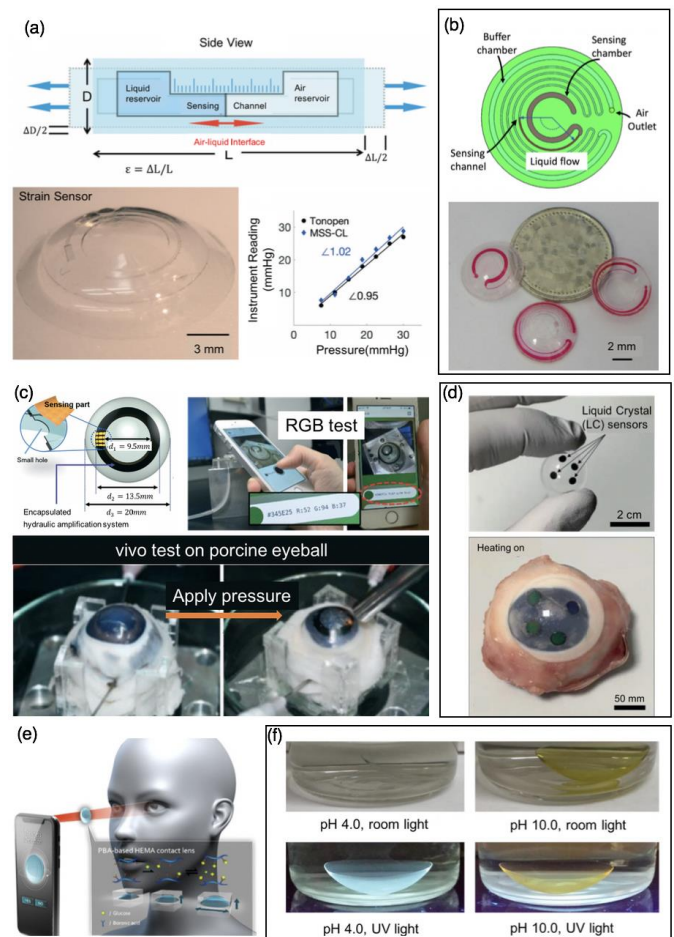

Fig. 2. Unpowered contact lens sensors: (a) microfluidic strain sensor. Reproduced with permission [60]. Copyright 2018, Royal Society of Chemistry. (b) microfluidic strain sensor with dyed red liquid. Reproduced with permission [62]. Copyright 2019, Elsevier. (c) photonic crystal pressure sensor. Reproduced with permission [63]. Copyright 2020, Royal Society of Chemistry. (d) TLC temperature sensor. Reproduced with permission [78]. Copyright 2019, Royal Society of Chemistry. (e) PBA-based HEMA glucose sensor. Reproduced with permission [82], Copyright 2018, Multidisciplinary Digital Publishing Institute (MDPI). (f) SiHG pH sensor. Reproduced with permission [83]. Copyright 2018, Elsevier.

glucose testing, where the contact lens was made of Phenylboronic acid (PBA)-based Hydroxyethyl methacrylate (HEMA) shown as Fig. 2(e) [82]. An image capturing smartphone was placed facing away from a red-light source through the proposed contact lens. Thickness is detected owing to the lens swelling due to the absorption of glucose into PBA material. This sensor noted a volume enlargement due to a growing glucose concentration, which provides a potential platform for non-enzyme glucose sensing. New silicone hydrogel (SiHG) contact lenses were proposed for pH sensing and detecting individual ionic species in tears (Fig. 2(f)). Tightly bound ion-sensitive fluorophores on SiHG lenses result in a wavelength-ratiometric shift, making it possible for pH value testing and lifetime-based chloride sensing [83]. In a low pH environment, SiHG sensors performed a bright blue emission, while a weaker yellow emission was detected in higher pH media. Meanwhile, in NaCl concentration changing from 0 mM to 100 mM, the SiHG pH sensor illustrated a fluorescence decrease with the increase of chloride concentration.

Although unpowered sensors using either biomedical, chemical, or optical principles achieve the wireless sensing for smart contact lenses, their accuracy cannot be guaranteed. Besides, these sensors are highly sensitive to their external environment, which means that extra care is needed for calibration. Consequently, in the next section, we will provide a review of the different powered sensors.

B. Powered Sensors

1) Electrical Sensors

Intraocular pressure sensing for glaucoma monitoring has been developed during the past two decades, where capacitive and piezo-resistive sensors have been extensively applied in electronic contact lenses for their characterization of pressure related to their electrical parameters to present a non-invasive approach.

a) Capacitive Sensing

Capacitive sensing is widely used for pressure detection and has been used in applications that include touchscreens, fingerprint sensors, and medical stethoscopes [84-87]. Here, when the permittivity values and overlapping area are constant, the applied pressure changes only the distance between the plates of the capacitive sensor, where non-capacitive parameters are converted into electrical signals. The distance between the upper and lower plate varies with the applied pressure, and the plate area may change with specific design as denoted using equation (2) [88],

$$C = \frac{\varepsilon_r \varepsilon_0 A}{d}, \qquad (2)$$

where, ε_r is the relative permittivity of the sandwiched substrate, which does not change in a contact lens sensor design. Similarly, ε_0 is the permittivity of free space (8.854×10^{-14} F/cm), A is the overlap area of the two plates, d is the gap distance between two plates.

This characterization method is particularly beneficial for IOP sensing in eye glaucoma detections [88-91] and researchers have used capacitive sensing in various electronic contact lens applications. According to Ali *et al.* a capacitive IOP sensor was fabricated with Poly-silicon/Air/Gold layers, on four corners of a 550 μm × 550 μm four slotted diaphragms [92], where the capacitance was linearized to the applied pressure. Moreover, Chiou *et al.* demonstrated a ring-shaped parallel plate capacitive sensor filled with poly-HEMA material, so that the application of pressure leads to a variation in the gap distance and plate area [93-95]. Their sensor was fabricated with Ti/Au plate material and encapsulated with Parylene-C, which detected pressure under a range of 16 mmHg to 30 mmHg with a sensitivity of 1.2239 pF/mmHg and consumed 100 μW power.

Apart from using readout circuitry, such as capacitance-to-digital converter (CDC) chips, inductively coupled coils contribute to intuitive and more straightforward design for output measurement. The resonant frequency changes as the capacitance variation through a connected inductive component, as explained via expression (3) [96],

$$f = \frac{1}{2\pi\sqrt{LC}}, \qquad (3)$$

where f is the resonant frequency, L is the total inductance of the sensing device, and C is the sensor capacitance. When the inductive and capacitive components are integrated into the electronic contact lenses, the frequency changes with the implied intraocular pressure. Chen *et al.* showed a linear relationship with a frequency response of 8 kHz/mmHg from 5mmHg to 45mmHg applied pressure [96].

b) Piezo-resistive sensing

Piezo-resistive electronic contact lens sensors transform the imposed force into electrical resistive signals, where the resistivity of the piezo-resistive material changes under the action of a force. Thus, the output electrical signal changes upon the application of a force.
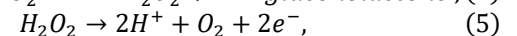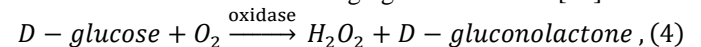
Piezo-resistive sensors are used to measure pressure through geometry alteration due to deformation in curvature. This curvature is a function of the sensor length (l) and cross-section area (A). Leonardi *et al.* added a sandwiched strain gauge resistive sensor between two polyimide plates, where the gauge is fabricated with platinum-titanium [97-99]. This resistive sensing concluded a sensitivity of 109 μV/mmHg and reproducibility of ± 0.2 mmHg with a linear regression coefficient $R^2 = 0.9935$. The contact lens was powered wirelessly through a loop antenna working under 27 MHz. The same structure was implemented commercially by Sensimed, where the "triggerfish" electronic lens sensor was used for measuring relative pressure changes in patients with glaucoma over 24 hours [100-103].

Another piezo-resistive sensing approach was fabricated with organic bi-layer (BL) films such as polycarbonate film, which were covered by an organic molecular conductor made of nanostructured crystals, where the resistive responses are at least three times larger than traditional metals. The sensitivity can be reduced to 1.5 Ω/mmHg [104, 105], but with limited power available from WPT, the contact lens would need low power measurement electronics such as Application Specific Integrated Circuit (ASIC) in reference [106].

2) Electrochemical Sensors

Biomarkers such as glucose, lactate, and hormones found in the blood can be detected from tears non-invasively. Electrochemical contact lens sensors are proposed due to their high sensitivity, excellent selectivity, and specific anti-interference ability, which provides a good sensing platform for idealized biosensors [66, 107-109].

The glucose sensor is a direct electron transfer sensor between the enzyme and the electrode, where the enzyme is attached directly to electrode holes on the polymer so that the active centre of the enzyme is close enough to react with the electrode, which benefits electron transfer. The main advantage of this sensor is that it does not need a receiver such as oxygen or any expensive medium, which avoids the interference caused by dissolved oxygen or the medium's complexity and limitation. Glucose contact lens sensors present both enzymatic and electrochemical reactions through glucose oxidase [65]:

$$D - glucose + O_2 \xrightarrow{\text{oxidase}} H_2O_2 + D - gluconolactone, (4)$$
$$H_2O_2 \rightarrow 2H^+ + O_2 + 2e^-, \qquad (5)$$

where hydrogen peroxide is produced through the reaction of glucose and oxygen, and electrons are released through electrochemical oxidation. Current flows lead by electrons migration can be measured, indicating the concentration of glucose in tears. In other words, the glucose level can be predicted by its linear relationship with current. In the electrochemical sensing system, the three-electrode layout

containing a working electrode (WE), reference electrode (RE), and a counter electrode (CE) is applied [110]. The differential voltage applied to WE and RE terminal guarantees electron movements, which varies from 400 mV to 700 mV in different case studies depending on electrode materials and chip design.

Chu et al. first proposed a glucose sensor on wearable contact lenses [66], where the 200 nm thick working electrode was made from Pt and the 300 nm thick reference/counter electrodes are fabricated with Ag/AgCl material on a 70 μm PDMS membrane (Fig. 3(a)). Glucose oxidase was immobilized with PMEH (Methacryloyloxyethyl phosphorylcholine (MPC) copolymerization with Ethylhexyl methacrylate (EHMA)) and the device was encapsulated with PDMS material. The glucose concentration was detected under a range of 0.03-5.0 mM with a correlation coefficient of 0.999 by applying a +400 mV constant differential voltage. In vitro testing on the rabbit eye was performed and the sensor formed an average current of 0.042 μA for a glucose concentration of 0.11 mM. In addition to different electrode materials, a loop glucose sensor applying the same three-electrode structure was proposed (Fig. 3(b)), which had a sensitivity of 240 $\mu Acm^{-2}mM^{-1}$ for a glucose concentration range from 0.1 mM to 0.6 mM. The glucose electrodes were made from Ti/Pd/Pt metal structure, which was wirelessly powered under 1.8 GHz with 3 μW power consumption [67-70].

Another approach was demonstrated with an enzymatic L-lactate sensor with the same structure and similar electrochemical reactions, where hydrogen peroxide was produced, and Pt electrons were generated with the same reaction. The same voltage difference was applied and the lactate sensor showed a high sensitivity of 53 $\mu Acm^{-2}mM^{-1}$ [107], as Fig. 3(c) illustrates. Keum et al. fabricated a glucose sensor (Fig. 3(d)) with chromium (Cr) and Pt as CE and WE terminal. Moreover, Ag/AgCl coated RE terminal on polyethylene terephthalate (PET) substrate encapsulated with a silicone hydrogel material, consuming 82 μW power including the sensor, integrated chip, and drug delivery system [108]. Their device showed a linear current increase from 0.41 μA to 3.12 μA with an increasing glucose concentration from 5 $mgdl^{-1}$ to 50 $mgdl^{-1}$, which also illustrated a good anti-interference of ascorbic acid, lactate, and urea in tears as well as stability of 63 days.

Donora et al. set up a series of experiments using spatiotemporal electrochemical sensing (Fig. 3(e)), on a contact lens, which was carefully designed with a strict power budget and reduced parasitic effects [109]. In the future, this will allow for wireless energy harvesting and integration with a flexible battery [111, 112]. Ferrocene methanol (FeMeOH) and Potassium chloride (KCl) concentration variation were measured from four electrode sensors on the contact lens, while the tear fluid flows across the cornea. This sensor successfully achieved fluid tracing under a high concentration, which lays the foundation for chemical measurement on the eye surface.

III. WIRELESS POWER TRANSFER IN CONTACT LENS SENSORS

An electronic contact lens with an antenna works as a receiver in wireless power and data transmission, which receives electromagnetic waves radiated from transmitting terminals on external devices [113]. The reflection coefficient is defined as the ratio of the magnitude of the reflected wave to the incident wave. The frequency at which the S_{11} value is minimum (-12 dB or less) is known as the resonant frequency. where a higher resonant frequency indicates a larger data capacity. A lower decibel value corresponds to a higher reflected power ratio. The bandwidth defines the ranges that the antenna can effectively radiate or receive energy (when $S_{11} < -10\ dB$). Thus, a larger bandwidth indicates a higher speed of potential data transmission [113]. The radiation resistance denotes the equivalent resistance which accounted for radiated power. The radiation efficiency is quantified by the ratio of the power radiated from the antenna relative to the power delivered to the antenna [114].

The frequency of existing electronic contact lenses varies widely from the Megahertz to the Gigahertz range, and from near field coupling to far-field radiation. Although antenna for lower frequencies provides less power loss, they usually require external impedance matching components that occupy the entire space of sensing circuits. Besides, the resonant frequency is inversely proportional to antenna size [114], although antennas applied in far-field present higher energy harvesting efficiency, they cause higher heat generation while transferring
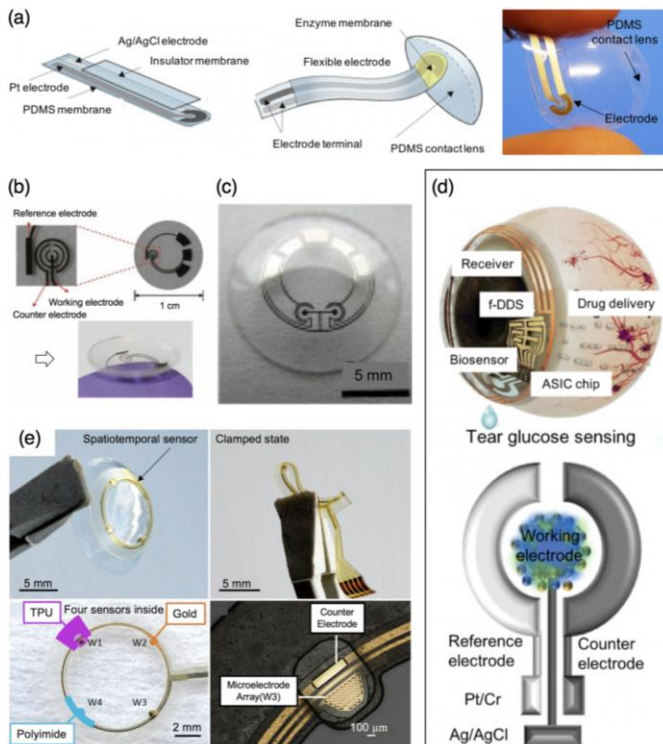
Fig. 3. Powered sensors: (a) three Ag/AgCl electrodes glucose sensor. Reproduced with permission [66]. Copyright 2010, Elsevier. (b) loop Ti/Pd/Pt glucose sensor. Reproduced with permission [69]. Copyright 2010, Elsevier. (c) Pt L-lactate sensor. Reproduced with permission [107]. Copyright 2011, Elsevier. (d) Pt/Cr glucose sensor integrated with drug delivery system with total 82 μW power consumption. Reproduced with permission [108]. Copyright 2020, American Association for the Advancement of Science (AAAS). (e) spatiotemporal sensor. Reproduced with permission [109]. Copyright 2019, Elsevier.

power. In terms of the energy consumption and wireless power delivery performance, near-field communication (NFC ~ 13.56 MHz) is optimized for electronic contact lens; However, in case of massive data transmission and higher data rate, mid-field (in the low GHz range) based wireless systems with well-controlled power loss are more suitable to satisfy the data transmission.

A. Loop Antenna

The challenges for antennas applying on electronic contact lenses are the size limitations under the donut-shaped area to avoid eyesight impedance while maintaining high power transferring ability. Researchers have made progress on various antenna shapes [115], where the loop antenna can be densely packed into a small area. Since it can be made from single or multiple turns of basic circular, rectangular, or triangular geometries, which are easy to fabricate [116-118]. Additionally, the interconnection between the loop antenna and the sensing circuit is relatively simple and clear, where electrical components are connected directly to the beginning and the end of the single loop.

According to the circumference size, L, relative to the wavelength (λ) of the received electromagnetic signal, the loop antenna can be divided into two categories: electrically large loop ($L \geq \lambda/10$), and small loop ($L < \lambda/10$) [114]. For an electronic contact lens, the magnetic loop antenna is suitable as the receiving antenna since the size of the designed antenna is generally constrained to be less than a tenth of the wavelength of the electromagnetic wave. The frequency applied on electronic contact lenses for loop antenna varies from 13.56 MHz High Frequency (HF) band to 5.8 GHz microwave band [94, 102, 112, 117, 119-121].

Fig. 4(a) shows an electronic contact lens working in the 915 MHz Industrial, Scientific, and Medical (ISM) band. The lens contained a sensor, chip, and antenna integration, where the resonant frequency was 920 MHz with 90 MHz bandwidth and -13 dB return loss. The power transfer capability can reach 100 µW from a maximum distance of 1 cm. Such an antenna working under the Ultra-high Frequency (UHF) frequency band can achieve both energy harvesting and data transmission simultaneously [94].

Generally, with different loop geometries, the resonant frequency also changes. Using an inner semi-circle design as shown in Fig. 4(b), both parasitic inductance and capacitance of the antenna increased and the frequency was reduced to 433 MHz, where the transferring distance is limited to 1 cm [119]. Lingley *et al.* proposed a loop antenna on an electronic contact lens with a micro-Fresnel lens for a future multi-pixel display application, depicted in Fig. 4(c). The in vitro testing frequency in that type showed a resonant point at 0.8-2.0 GHz where the antenna was fabricated with 0.5 mm loop width and 5 mm antenna radius [117]. However, that antenna was only used for powering an integrated LED with a higher power of 117 µW and a more extended energy harvesting distance of 2 cm.

Cheng et al. designed a rectenna using a combination of Gold (Au) and Titanium (Ti) as the antenna material, as illustrated in Fig. 4(d). Their design increased the resonant frequency to 5.8 GHz, where the data transfer capacity was increased, as well as the power delivery performance. The bandwidth for higher frequency bands, such as 5.8 GHz, was found to be 2 GHz at -
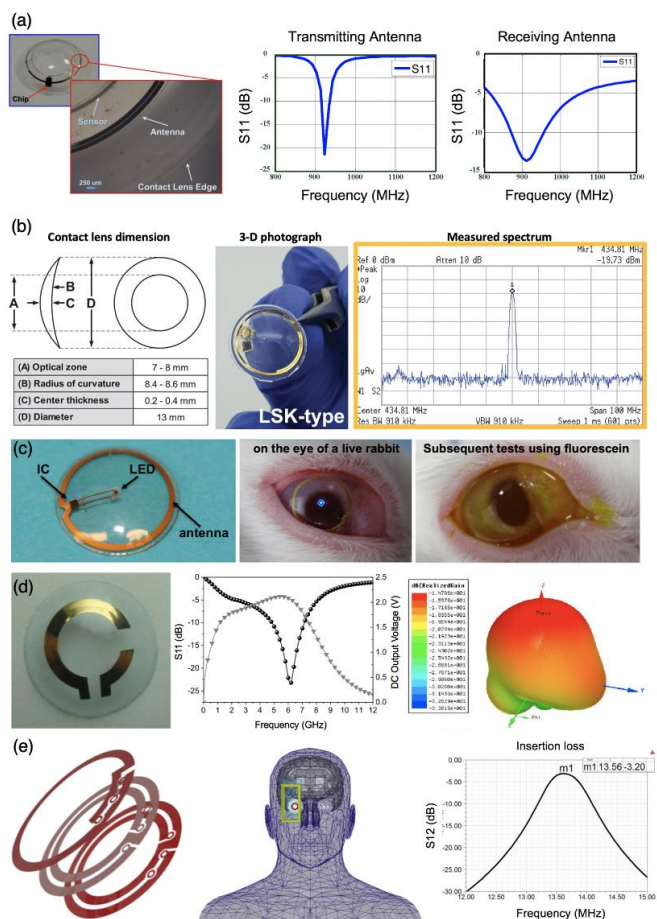

Fig. 4. Loop antenna on smart contact lens: (a) working under $920 \, \mathrm{MHz}$ Reproduced with permission [94]. Copyright 2017, MDPI. (b) with inner semi-circle designed antenna working under 433 MHz. Reproduced with permission [119]. Copyright 2019, IEEE. (c) integrated with pixel LED working under 0.8-2.0 GHz. Reproduced with permission [117]. Copyright 2011, Institute of Physics. (d) working under 5.8 GHz. Reproduced with permission [120]. Copyright 2013, IEEE. (e) 3-layers loop antenna working under 13.56 MHz. Reproduced with permission [121]. Copyright 2015, IEEE.

10 dB, since the working frequency shifted to the Gigahertz level. However, the simulated SAR distribution presented 514 W/Kg under 1 W power transfer, which constrained the power delivery to 3.1 mW due to the ANSI/IEEE SAR regulations [122]. As the far-field radiation pattern shows in Fig. 4(d), a single loop antenna could be highly directional [120].

Since a single loop in the constrained contact lens size may not generate the desired power for system operation, another transformation of loop antenna such as multiple layers of circular loop shapes also present variations in resonant frequency [121], where the receiving antenna was designed as a combination of three layers loop antenna, as shown in Fig. 4(e). The assembly of multiple layers that can lower the resonant frequency to 13.56 MHz, which achieved Near-Field Communication (NFC) with NFC-enabled smartphone.

The conventional small loop antenna is mainly used as a receiver antenna since the impedance mismatch is a vital problem. Due to its linear polarization characteristic, the position of the loop antenna during the data transferring process requires to be considered. Moreover, for wearable devices such as electronic contact lenses, the loop antenna still has relatively

low radiation resistance results in low radiation efficiency [114]. Although the radiation resistance can be enlarged by multiturn loops and the polarization direction can be changed by tuning antenna with different designs and frequencies [114], the loop antenna offers fewer designing flexibilities compared to other antenna shapes.

B. Spiral Antenna

The spiral antenna has been verified as applicable for health monitoring since the spiral shape can be altered easily while maintaining miniaturized geometry [123]. As compared to the linearly polarized loop antenna, the spiral antenna can receive signals in any direction due to its circular polarization [114]. One variant of the spiral design, the Archimedean antenna, commonly has two arms that wind around one another [125, 126], and so could obstruct the eye pupil if used in an electronic contact lens, thus, the one-armed spiral antenna is more feasible to fit the limited space. Since the current distribution is rapidly attenuated along the arm of the spiral antenna, cutting off the antenna arm at the point where the current value approaches zero can be used for tuning the resonant frequency, so that the length of the antenna arm can be lengthened and shortened to meet the requirements of the working frequency segment of the antenna [124]. Apart from the circular polarization which contributes to both transmitting and receiving antenna, the spiral antennas applying on the Gigahertz range possess high bandwidth [114]. The broadband of the spiral antenna enables high power transfer and faster data transmission, which provides a platform for high quality simultaneous wireless information and power transferability [127, 128].

The working frequency of the single-arm spiral antenna on the electronic contact lens varies from 13.56 MHz to 4.3 GHz, covering high frequency and microwave frequency bands [129-132]. In terms of simultaneous energy harvesting and data transmission, the spiral shape antenna can be confined in the donut gap between the eye pupil and the outer contact lens circle, as shown in Fig. 5(a). This antenna operates under the 2.4 GHz ISM band with 90 MHz bandwidth and -28 dB return loss [129]. The simulated SAR was controlled using 0.4 W/Kg for 0.1 W of transmitted power. To have natural eyesight, the inner radius of the spiral antenna was designed to 4 mm and the antenna had three turns with a 0.2 mm antenna wire width. As the 3-D polar plot illustrated, the Archimedean spiral antenna radiated outward from the contact lens, enabling the power and data transmission on each position in front of the device. However, for circular polarization under 2.45 GHz antenna, the presence of a back-lobe may cause damage to the human body, and a load must be positioned at the end of the arm to avoid wave reflection, since the current attenuation decrease slowly along the spiral arm, which could not guarantee the frequency independence of Archimedean spiral antenna [114].

Due to the relatively wide pressure surface and uniform pressure distribution, the spiral antenna can be used for intraocular pressure sensing, since the resonant frequency varies due to changes in geometry that are caused by applied pressure. As Fig. 5(b) shows, an intraocular sensor with an inner implant tube was fabricated by Lin *et al.* [130]. The capacitive sensor was in the centre of the spiral antenna, and the antenna was placed outside the cornea for maintaining electromagnetic properties during pressure variation. Both inductive and
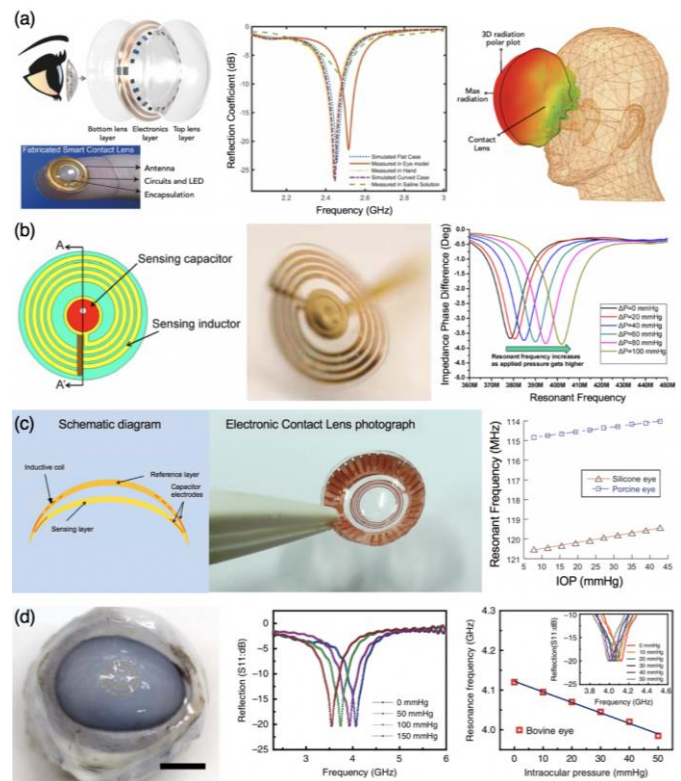

Fig. 5. Spiral antenna on smart contact lens: (a) with rectifying circuits works under 2.4 GHz. Reproduced with permission [129], Copyright 2020, WILEY-VCH. (b) with sensing capacitor under 379 MHz–402 MHz varying frequency. Reproduced with permission [130]. Copyright 2012, IEEE. (c) with IOP sensing works under 120 MHz frequency. Reproduced with permission [131]. Copyright 2013, Elsevier. (d) made of Au/Ti material works under 4.1 GHz. Reproduced with permission [132]. Copyright 2017, Springer Nature. Scale bar: 1cm.

capacitive components were made from a combination of Au and Ti. Thus, as the applied pressure increased the device provided a resonant frequency shift from 379 MHz to 402 MHz. A similar sensing device with copper was developed as in Fig. 5(c). The intraocular sensor was composed of two capacitive layers and a spiral antenna acted as a simultaneous power transfer and sensing unit, where the spiral antenna was coated in hard silicone elastomer as the reference layer [131]. By applying pressure on the contact lens, the resonant frequency shifted from 119 MHz to 120 MHz, 114 MHz to 115 MHz with the pressure decreasing on silicon and porcine eye, respectively. Additionally, the maximum reading distance reached 25 mm.

Using silver nanowires (AgNWs) as the antenna material (Fig. 5(d)) significantly enhanced the contact lens transparency and the resonant frequency shifted to 4.1 GHz with the spiral antenna for powering the integrated glucose sensor. However, as Fig. 5(d) illustrates, as an IOP sensor, a flexible silicone elastomer (Ecoflex) layer was placed between two inductive components where the intraocular-pressure-caused corneal radius curvature change can be detected from the working frequency [132]. This is similar to [123] in which two inductive coils are separated by a layer of styrene-butadiene-styrene (SBS) elastomer, for a wrist-wearable pulse sensor. Generally, the resonant frequency of this device varied from 3.4 GHz and 4.3 GHz when the pressure was reduced from 150 mmHg to zero, and it presented a narrower frequency variation on the Bovine eye test which was around 4 GHz to 4.1 GHz. The spiral

antenna in that case delivered power and transferred data in the GHz level, which processed a high bandwidth and can still be applied for IOP sensing due to its even compression characteristic.

C. Nanomaterials

Although stretchability in deformation can be an advantage in many instances, transparency is also a vital feature for bio-integrated applications, especially electronic contact lenses, where transparency can provide more available space for the applied antenna. Carefully choosing the encapsulation material is therefore important to achieve transparency [133, 134]. Since traditional conductive materials are confined to donut shape due to their opacification, nanomaterials that are small-sized under 100 nm have remarkably low light absorption [135]. When the particle size is reduced to the nanometre scale, the acoustic, optical, electrical, magnetic, and thermal properties will take on new characteristics.

Among various nanomaterials, graphene, and silver nanowires (AgNW) process high electron mobility with low resistivity and high conductivity, which has less heat generation and consumes less energy while allowing highly conductive characteristics. Additionally, graphene and AgNW have excellent light transmittance with around 90% photon transmissivity. As Fig. 6(a) shows, a coplanar waveguide (CPW)-fed graphene monopole antenna was fabricated with graphene material on a PET–substrate to allow a totally transparent device [136]. That monopole antenna demonstrated two resonant frequencies at 10 GHz and 19 GHz, where the S_{11} is around -14 dB at 10 GHz. Different numbers of graphene layers were applied to test its radiant characteristics. Typically, increasing the number of graphene layers from 3 to 8 resulted in higher light attenuation and poorer light transmittance. However, the conductivity increased with the increased layer number. Besides, the radiation efficiency reached 40-55% with 8-layer graphene material, the resonant frequency of monopole antenna with graphene material significantly shifted to C-band (5.8 GHz) and X-band (10.7-12.2 GHz) with Ultra-wideband (UWB). As the radiation pattern shown in Fig. 6(a), that antenna demonstrated omnidirectional radiation whose emitted power are equal along with all the directions.

Although graphene materials can help to achieve higher bandwidth, the additional cost prevents such devices from reaching the production level. However, mixing AgNW with graphene could be an alternative to achieve a reasonable price trade-off. Large *et al.* from the University of Sussex has developed an attractive material to replace Indium Tin Oxide (ITO), which consists of a mixture of silver nanowires and graphene [137]. Since only a fraction of the nanowires is used to get the properties of ITO, that hybrid material is relatively cheap. Graphene acts as a link to the nanowires, which makes nanowires less densely connected. Adding graphene to the nanofilament spray network through thin film deposition is significantly less expensive than the AgNW generation itself, which opens the potential for the material to capture market share in transparent conductors.

The mixture of AgNW and graphene was also used for antenna design in electronic contact lenses, as shown in Fig. 6(b). A spiral shape antenna was fabricated with AgNW and graphene material, whose optical transmittance was above 80%
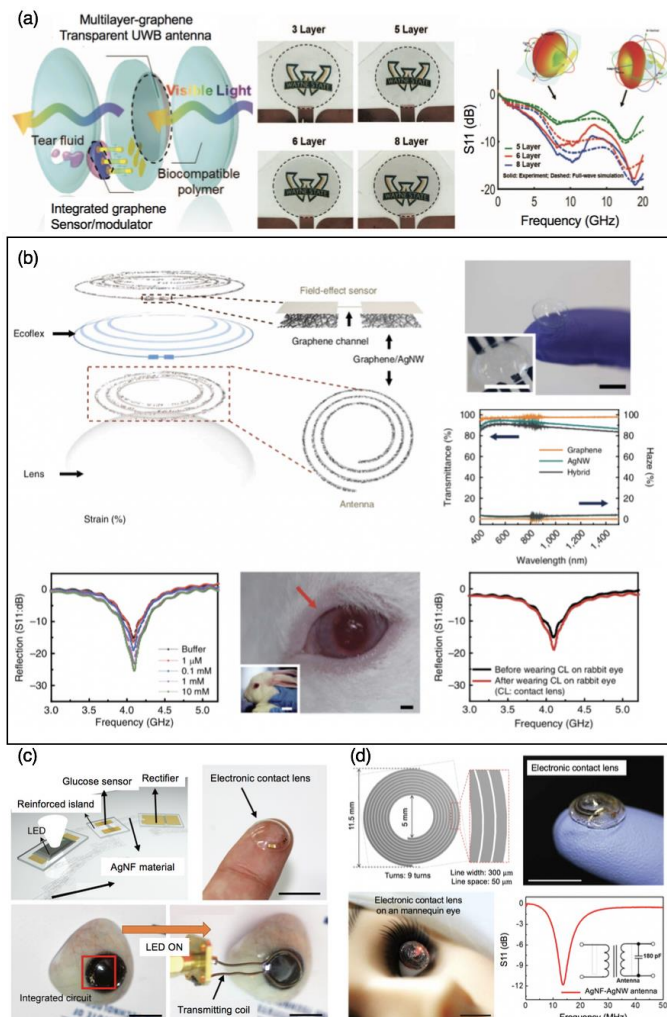

Fig. 6. Contact lens antenna generated with: (a) graphene material of monopole antenna shape. Reproduced with permission [136], Copyright 2016, IEEE. (b) graphene-AgNW hybrid of spiral antenna shape. Reproduced with permission [132]. Copyright 2017, Springer Nature. Scale bars: 1 cm. (c) AgNF of single-loop antenna shape. Reproduced with permission [143]. Copyright 2018, AAAS. Scale bars: 1 cm. (d) AgNW-AgNF hybrid of special antenna shape. Reproduced with permission [145]. Copyright 2019, AAAS. Scale bars: 1 cm.

and haze spectra below 10% from a wavelength sweep of 400-1,400 nm. This hybrid structure was used for both antenna and electrode fabrication due to its negligible transconductance, where the interconnection was fabricated from a graphene channel enabling glucose-sensing [138-141]. As a result of wireless power transfer for glucose oxidase sensors, the graphene-AgNW hybrid structure delivered power under 4.1 GHz with 400 MHz. Moreover, the reflectivity increased with higher glucose concentrations, whereas the graphene sheet resistance decreased due to higher glucose binding. Graphene-AgNW hybrids not only reduce the production cost but also the energy demand during the fabrication process.

Another choice of antenna nanomaterial is pure silver nanowires or nanofibers, where the optical transmittance properties are maintained and the film fabrication process is less complicated [142]. As shown in Fig. 6(c), the glucose sensor was fabricated from graphene channels due to its high electron mobility which contributes to higher sensitivity [143]. However, the single loop antenna and interconnection consisted of pure 1-D ultralong silver nanofibers (AgNFs). The antenna, which has

TABLE II
STATE-OF-ART ANTENNA COMPARISON IN CONTACT LENS SENSORS

Antenna Type	Antenna Material	Substrate Type	Operating Frequency	Power Transferring Performance				Efficiency (%)	Test Condition	Year	Ref.
				Bandwidth	S11(dB)	Distance	Power				
Dipole	Cu	-	850MHz	50MHz	-23.98	-	-	47	in air	2018	[115]
Loop 3-layers	-	Polymer	13.56MHz	-	less than -10	2cm	-	49	in saline solution	2015	[121]
Monopole	Graphene	PET	10 GHz & 19 GHz	-	-14@10 GHz	-	-	136	in air	2016	[136]
Single-loop	AgNF	Elastic polymer (elastofilcon A)	50MHz	-	-	5mm	-	21.5	on a live rabbit eye	2018	[143]
Single-loop	Zn	Commercialized lens (PureVision2 lenses)	13.56MHz	-	-	10mm	74μW	17.6	on a porcine eye	2019	[116]
Single-loop	Au/Ti	HEMA	920MHz	90MHz	-13	1cm	110μW	-	on a porcine eye	2016	[94]
Single-loop	Au/Ti	Parylene-C	5.8GHz	2GHz	-23	-	2.2mW	35.1	on a porcine eye	2013	[120]
Single-loop	Au	PET	433MHz	-	-19.73	1cm	0.49μW	-	in air	2019	[119]
Single-loop	Au	PET	0.8−2.0GHz	-	-	2cm	117μW	-	on a live rabbit eye	2016	[117]
Spiral	AgNW	Commercialized lens	4.1GHz	400MHz	-20	-	-	-	on bovine eye	2017	[132]
Spiral	AgNW/AgNF	Elastic polymer (elastofilcon A)	13.56MHz	-	-	5mm	0.36mW	-	in vivo	2019	[145]
Spiral	Cu	PDMS	2.4GHz	90MHz	-28	-	-	-	in saline solution	2019	[129]
Square-Loop	Cu	Commercialized lens	4.1GHz	-	-	10cm	-	-	in air	2018	[38]

a 12 mm diameter and 0.5 mm wire width, has a reduced working frequency of 50 MHz to switch on the attached LED pixel with 21.5% power transfer efficiency. Instead of Reactive Ion Etching (RIE), silver nanofibers (AgNF) can be electrospun on a prepared substrate with rectifier circuit manufacture simultaneously through wet etching, which largely simplifies the fabrication process. That single loop antenna with AgNF material can transfer power from a 5 mm distance and the SAR value was controlled below 1.399 W/Kg.

Since individual AgNW or AgNF have high flexibility and stretchability that present poor mechanical stability [144], especially under antenna application where intraocular mechanical deformations largely alter the antenna architecture and electromagnetic properties of the device, the compound of ultralong AgNFs and fine AgNWs with special spiral construction can be applied to prevent the device from mechanical deformations as shown in Fig. 6(d). In terms of that spiral generation, the sheet resistance decreased significantly with the area fraction of AgNF while the device demonstrated a lower optical transmittance. Through the trade-off between optical and electrical characteristics, the spiral shape antenna was fabricated with an outer diameter of 11.5 mm and 5 mm inner diameter, where the transparency of AgNW-AgNF hybrid structured gained more available space on electronic contact lens for wireless power transfer unit [145]. The 300 µm spiral wire consisted of AgNW and the 50 µm inner space between spiral lines was filled with AgNF, with which the antenna can maintain its spiral characteristics when inevitable strain is applied. The antenna worked in the 13.56 MHz NFC frequency band with a 180 pF matching capacitance, whose transfer distance reached 5 mm with 0.36 mW power to switch on the load LED.

Nanomaterials used in electronic contact lenses are of fundamental as well as practical importance. On the theoretical side, the exploration of nanohybrid mechanisms broadens our horizons of micromechanical systems and biomedically wearable devices. At the practical level, nanostructured materials provide transparent flexibility and better electrical properties, which benefits energy harvesting and data transmission antennas on wearable devices. State-of-art antennas applied on electronic contact lenses are compared in Table II, it is obvious that spiral shape antennas resonant in higher frequency bands than single loop antennas. The addition of nanomaterials such as graphene and silver nanofibers have significant frequency shifts, higher bandwidth, and higher power transfer efficiency.

IV. CONCLUSION AND FUTURE PERSPECTIVES

Electronic contact lenses have been used for disease monitoring, where their long-term stability as well as their biocompatibility are considered crucial. Notably, the electronic contact lens platform is promising for future drug therapies and treatments. Some contact lens sensors are inherently powered via stimuli from the surrounding environment (such as temperature, pH variations, or chemical reactions), while others used for intraocular pressure and glucose detections are powered via novel antenna designs. Electronic contact lenses using various antenna shapes and materials proves the possibility of antenna application on different wearable devices. Some of the open research questions include:

A. Heat Control

The control of heat generation from the electronics and the antenna is significant for electronic contact lenses, since all the components are placed inside the eye and contact directly with tears fluids. Sufficient thermal tests are of vital importance to control the lenses within an appropriate temperature range. Antenna applied in higher frequencies will present more risks

on heat damage to human body. Nevertheless, an experimental investigation on SAR is needed for exposure control under high power density and high frequency.

B. Hybrid Nanomaterials

Future research on antenna size, biocompatible encapsulation layers, bandwidth, and radiation efficiencies is necessary in terms of surrounding influence on electronic contact lenses antennas. Whilst hybrid nanomaterials have included graphene or silver nanomaterials to achieve high optical transparency and electrical conductivity. Therefore, Graphene-AgNW hybrids may be the most viable alternative for transparent electronic devices, which is better than other competitors in terms of price and performance.

C. Flexible and Stretchable Sensors

Flexibility and stretchability are promising research directions that have already been applied for other sensitive stretchable body areas such as the brain or heart. Stretchable structures applied to contact lenses can be used as flexible sensors and antennas with stronger electromagnetic performance. By optimizing stability, sensitivity and reading distance based on various power transfer methods and structures, further research combining specific sensors and readout circuits could also be conducted to determine the effectiveness of electronic contact lenses as non-invasive biomedical sensors.

REFERENCES

[1] D. Son, J. Lee, S. Qiao, R. Ghaffari, J. Kim, J. E. Lee, C. Song, S. J. Kim, D. J. Lee, S. W. Jun, S. Yang, M. Park, J. Shin, K. Do, M. Lee, K. Kang, C. S. Hwang, N. Lu, T. Hyeon, and D. H. Kim, "Multifunctional wearable devices for diagnosis and therapy of movement disorders," *Nat Nanotechnol,* vol. 9, no. 5, pp. 397-404, May, 2014.

[2] M. A. Case, H. A. Burwick, K. G. Volpp, and M. S. Patel, "Accuracy of smartphone applications and wearable devices for tracking physical activity data," *JAMA,* vol. 313, no. 6, pp. 625-6, Feb 10, 2015.

[3] M. Haghi, K. Thurow, and R. Stoll, "Wearable Devices in Medical Internet of Things: Scientific Research and Commercially Available Devices," *Healthc Inform Res,* vol. 23, no. 1, pp. 4-15, Jan, 2017.

[4] S. Mann, "Wearable computing: A first step toward personal imaging," *Computer,* vol. 30, no. 2, pp. 25-32, 1997.

[5] X. Liang, H. Li, W. Wang, Y. Liu, R. Ghannam, F. Fioranelli, and H. Heidari, "Fusion of Wearable and Contactless Sensors for Intelligent Gesture Recognition," *Advanced Intelligent Systems,* vol. 1, no. 7, pp. 1900088, 2019.

[6] R. M. Al-Eidan, H. Al-Khalifa, and A. M. Al-Salman, "A review of wrist-worn wearable: Sensors, models, and challenges," *Journal of Sensors,* vol. 2018, no. 5853917, pp. 1-20, Dec, 2018.

[7] S. Yao, A. Myers, A. Malhotra, F. Lin, A. Bozkurt, J. F. Muth, and Y. Zhu, "A wearable hydration sensor with conformal nanowire electrodes," *Advanced healthcare materials,* vol. 6, no. 6, pp. 1601159, 2017.

[8] H. Ye, M. Malu, U. Oh, and L. Findlater, "Current and future mobile and wearable device use by people with visual impairments." pp. 3123-3132.

[9] Y. Gao, H. Ota, E. W. Schaler, K. Chen, A. Zhao, W. Gao, H. M. Fahad, Y. Leng, A. Zheng, and F. Xiong, "Wearable microfluidic diaphragm pressure sensor for health and tactile touch monitoring," *Advanced Materials,* vol. 29, no. 39, pp. 1701985, 2017.

[10] F. Wu, H. Zhao, Y. Zhao, and H. Zhong, "Development of a wearable-sensor-based fall detection system," *International journal of telemedicine and applications,* vol. 2015, no. 576364, 2015.

[11] T. Ishikawa, Y. Hyodo, K. Miyashita, K. Yoshifuji, Y. Komoriya, and Y. Imai, "Wearable motion tolerant ppg sensor for instant heart rate in daily activity," *Conf. Biomed. Eng. Sys. Tech.*, pp. 126-133, 2017.

[12] W. Gao, S. Emaminejad, H. Y. Y. Nyein, S. Challa, K. Chen, A. Peck, M. Fahad, H. Ota, H. Shiraki, D. Kiriya, D. H. Lien, G. A. Brooks, R. W. Davis, and A. Javey, "Fully integrated wearable sensor arrays for multiplexed in situ perspiration analysis," *Nature,* vol. 529, no. 7587, pp. 509-514, Jan 28, 2016.

[13] S. J. Morris, "A shoe-integrated sensor system for wireless gait analysis and real-time therapeutic feedback," Massachusetts Institute of Technology, 2004.

[14] M. Li, J. Xiao, J. Wu, R.-H. Kim, Z. Kang, Y. Huang, and J. A. Rogers, "Mechanics analysis of two-dimensionally prestrained elastomeric thin film for stretchable electronics," *Acta Mechanica Solida Sinica,* vol. 23, no. 6, pp. 592-599, 2010.

[15] A. J. Bandodkar, J.-M. You, N.-H. Kim, Y. Gu, R. Kumar, A. V. Mohan, J. Kurniawan, S. Imani, T. Nakagawa, and B. Parish, "Soft, stretchable, high power density electronic skin-based biofuel cells for scavenging energy from human sweat," *Energy & Environmental Science,* vol. 10, no. 7, pp. 1581-1589, 2017.

[16] W. H. Yeo, Y. S. Kim, J. Lee, A. Ameen, L. Shi, M. Li, S. Wang, R. Ma, S. H. Jin, and Z. Kang, "Multifunctional epidermal electronics printed directly onto the skin," *Advanced materials,* vol. 25, no. 20, pp. 2773-2778, 2013.

[17] A. M. Hussain, F. A. Ghaffar, S. I. Park, J. A. Rogers, A. Shamim, and M. M. Hussain, "Metal/polymer based stretchable antenna for constant frequency far‐field communication in wearable electronics," *Advanced Functional Materials,* vol. 25, no. 42, pp. 6565-6575, 2015.

[18] Y. Huang, Y. Wang, L. Xiao, H. Liu, W. Dong, and Z. Yin, "Microfluidic serpentine antennas with designed mechanical tunability," *Lab on a Chip,* vol. 14, no. 21, pp. 4205-4212, 2014.

[19] M. Chen, Y. Ma, J. Song, C.-F. Lai, and B. Hu, "Smart clothing: Connecting human with clouds and big data for sustainable health monitoring," *Mobile Networks and Applications,* vol. 21, no. 5, pp. 825-845, 2016.

[20] C. Gonçalves, A. Ferreira da Silva, J. Gomes, and R. Simoes, "Wearable e-textile technologies: A review on sensors, actuators and control elements," *Inventions,* vol. 3, no. 1, pp. 14, 2018.

[21] N. T. Sahin, N. U. Keshav, J. P. Salisbury, and A. Vahabzadeh, "Second version of google glass as a wearable socio-affective aid: positive school desirability, high usability, and theoretical framework in a sample of children with autism," *JMIR human factors,* vol. 5, no. 1, pp. e1, 2018.

[22] W. Hsu, "Eyeglasses frame," Google Patents, 2016.

[23] A. Syberfeldt, O. Danielsson, and P. Gustavsson, "Augmented reality smart glasses in the smart factory: Product evaluation guidelines and review of available products," *Ieee Access,* vol. 5, pp. 9118-9130, 2017.

[24] A. Aliverti, "Wearable technology: role in respiratory health and disease," *Breathe,* vol. 13, no. 2, pp. e27-e36, 2017.

[25] S. Patel, H. Park, P. Bonato, L. Chan, and M. Rodgers, "A review of wearable sensors and systems with application in rehabilitation," *Journal of neuroengineering and rehabilitation,* vol. 9, no. 1, pp. 1-17, 2012.

[26] K. N. Bocan, and E. Sejdić, "Adaptive transcutaneous power transfer to implantable devices: A state of the art review," *Sensors,* vol. 16, no. 3, pp. 393, 2016.

[27] E. Ghafar-Zadeh, "Wireless integrated biosensors for point-of-care diagnostic applications," *Sensors,* vol. 15, no. 2, pp. 3236-3261, 2015.

[28] S. R. Corrie, J. Coffey, J. Islam, K. Markey, and M. Kendall, "Blood, sweat, and tears: developing clinically relevant protein biosensors for integrated body fluid analysis," *Analyst,* vol. 140, no. 13, pp. 4350-4364, 2015.

[29] P. J. Soh, G. A. Vandenbosch, M. Mercuri, and D. M.-P. Schreurs, "Wearable wireless health monitoring: Current developments, challenges, and future trends," *IEEE Microwave Magazine,* vol. 16, no. 4, pp. 55-70, 2015.

[30] J. Pandey, Y.-T. Liao, A. Lingley, B. Parviz, and B. Otis, "Toward an active contact lens: Integration of a wireless power harvesting IC," *Conf. Biomed. Circuits. Syst.*, pp. 125-128, Nov, 2009.

[31] C.-C. Peng, M. T. Burke, B. E. Carbia, C. Plummer, and A. Chauhan, "Extended drug delivery by contact lenses for glaucoma therapy," *Journal of controlled release,* vol. 162, no. 1, pp. 152-158, 2012.

[32] T. Eggers, J. Draeger, K. Hille, C. Marschner, P. Stegmaier, J. Binder, and R. Laur, "Wireless intra-ocular pressure monitoring system integrated into an artificial lens," *Conf. Microtech-nologies in Medicine and Biology.*, pp. 466-469, Oct, 2000.

[33] C. G. Parkin, C. Graham, and J. Smolskis, "Continuous Glucose Monitoring Use in Type 1 Diabetes: Longitudinal Analysis Demonstrates Meaningful Improvements in HbA1c and Reductions in Health Care Utilization," *Journal of Diabetes Science and Technology,* vol. 11, no. 3, pp. 522-528, 2017.

[34] J. Dong, Z. A. Syed, K. Fan, A. F. Yahya, and S. A. Melki, "Potential Savings from Visit Reduction of Continuous Intraocular Pressure

Monitoring," *J Curr Glaucoma Pract,* vol. 12, no. 2, pp. 59-63, May-Aug, 2018.

[35] R. R. Holman, S. K. Paul, M. A. Bethel, D. R. Matthews, and H. A. W. Neil, "10-year follow-up of intensive glucose control in type 2 diabetes," *New England journal of medicine,* vol. 359, no. 15, pp. 1577-1589, 2008.

[36] C. Lin, B. Pratt, M. Honikel, A. Jenish, B. Ramesh, A. Alkhan, and J. T. La Belle, "Toward the development of a glucose dehydrogenase-based saliva glucose sensor without the need for sample preparation," *Journal of diabetes science and technology,* vol. 12, no. 1, pp. 83-89, 2018.

[37] S. H. Lim, R. Martino, V. Anikst, Z. Xu, S. Mix, R. Benjamin, H. Schub, M. Eiden, P. A. Rhodes, and N. Banaei, "Rapid diagnosis of tuberculosis from analysis of urine volatile organic compounds," *ACS sensors,* vol. 1, no. 7, pp. 852-856, 2016.

[38] K. Hayashi, S. Arata, G. Xu, S. Murakami, C. D. Bui, T. Doike, M. Matsunaga, A. Kobayashi, and K. Niitsu, "A 385 mu m x 385 mu m 0.165 V 0.27 nW Fully-Integrated Supply-Modulated OOK CMOS TX in 65nm CMOS for Glasses-Free, Self-Powered, and Fuel-Cell-Embedded Continuous Glucose Monitoring Contact Lens," *2018 Ieee Biomedical Circuits and Systems Conference (Biocas): Advanced Systems for Enhancing Human Health*, pp. 379-382, 2018.

[39] D. Harvey, N. W. Hayes, and B. Tighe, "Fibre optics sensors in tear electrolyte analysis: Towards a novel point of care potassium sensor," *Contact Lens and Anterior Eye,* vol. 35, no. 3, pp. 137-144, 2012.

[40] K. Mitsubayashi, and T. Arakawa, "Cavitas sensors: Contact lens type sensors & mouthguard sensors," *Electroanalysis,* vol. 28, no. 6, pp. 1170-1187, 2016.

[41] J. P. Gilbard, "Human tear film electrolyte concentrations in health and dry-eye disease," *International ophthalmology clinics,* vol. 34, no. 1, pp. 27-36, 1994.

[42] C. R. Taormina, J. T. Baca, S. A. Asher, J. J. Grabowski, and D. N. Finegold, "Analysis of tear glucose concentration with electrospray ionization mass spectrometry," *Journal of the American Society for Mass Spectrometry,* vol. 18, no. 2, pp. 332-336, 2007.

[43] L. G. Carney, T. F. Mauger, and R. M. Hill, "Buffering in human tears: pH responses to acid and base challenge," *Investigative ophthalmology & visual science,* vol. 30, no. 4, pp. 747-754, 1989.

[44] A. Cancarini, J. Fostinelli, L. Napoli, M. Gilberti, P. Apostoli, and F. Semeraro, "Trace elements and diabetes: assessment of levels in tears and serum," *Experimental eye research,* vol. 154, pp. 47-52, 2017.

[45] A. Kijlstra, S. Jeurissen, and K. Koning, "Lactoferrin levels in normal human tears," *British Journal of Ophthalmology,* vol. 67, no. 3, pp. 199-202, 1983.

[46] V. Ng, and P. Cho, "The relationship between total tear protein concentrations determined by different methods and standards," *Graefe's archive for clinical and experimental ophthalmology,* vol. 238, no. 7, pp. 571-576, 2000.

[47] H. Hashemi, A. Kashi, A. Fotouhi, and K. Mohammad, "Distribution of intraocular pressure in healthy Iranian individuals: the Tehran Eye Study," *British journal of ophthalmology,* vol. 89, no. 6, pp. 652-657, 2005.

[48] A. Rastegar, and M. Soleimani, "Hypokalaemia and hyperkalaemia," *Postgrad Med J,* vol. 77, no. 914, pp. 759-64, Dec, 2001.

[49] A. Alghadyan, M. Aljindan, A. Alhumeidan, G. Kazi, and R. McMhon, "Lacrimal glands in cystic fibrosis," *Saudi J Ophthalmol,* vol. 27, no. 2, pp. 113-116, Apr, 2013.

[50] L. S. Feiler, G. Smolin, M. Okumoto, and D. Condon, "Herpetic keratitis in zinc-deficient rabbits," *Invest Ophthalmol Vis Sci,* vol. 22, no. 6, pp. 788-95, Jun, 1982.

[51] Y. Danjo, M. Lee, K. Horimoto, and T. Hamano, "Ocular surface damage and tear lactoferrin in dry eye syndrome," *Acta Ophthalmol (Copenh),* vol. 72, no. 4, pp. 433-7, Aug, 1994.

[52] C. Terres-Martos, M. Navarro-Alarcon, F. Martin-Lagos, G. d. l. S. H. Lopez, V. Perez-Valero, and M. C. Lopez-Martinez, "Serum zinc and copper concentrations and Cu/Zn ratios in patients with hepatopathies or diabetes," *J Trace Elem Med Biol,* vol. 12, no. 1, pp. 44-49, Mar, 1998.

[53] J. Murube, "Basal, reflex, and psycho-emotional tears," *Ocul Surf,* vol. 7, no. 2, pp. 60-66, Apr, 2009.

[54] N. V. U. Hohenstein-Blaul, S. Funke, and F. H. Grus, "Tears as a source of biomarkers for ocular and systemic diseases," *Experimental Eye Research,* vol. 117, pp. 126-137, Dec, 2013.

[55] N. M. Farandos, A. K. Yetisen, M. J. Monteiro, C. R. Lowe, and S. H. Yun, "Contact lens sensors in ocular diagnostics," *Adv Healthc Mater,* vol. 4, no. 6, pp. 792-810, Apr 22, 2015.

[56] N. J. Van Haeringen, "Clinical biochemistry of tears," *Surv Ophthalmol,* vol. 26, no. 2, pp. 84-96, 1981.

[57] A. Mann, and B. Tighe, "Contact lens interactions with the tear film," *Exp Eye Res,* vol. 117, pp. 88-98, Dec, 2013.

[58] A. Kunzmann, B. Andersson, T. Thurnherr, H. Krug, A. Scheynius, and B. Fadeel, "Toxicology of engineered nanomaterials: focus on biocompatibility, biodistribution and biodegradation," *Biochim Biophys Acta,* vol. 1810, no. 3, pp. 361-73, Mar, 2011.

[59] W. Mokwa, and U. Schnakenberg, "Micro-transponder systems for medical applications," *Ieee Transactions on Instrumentation and Measurement,* vol. 50, no. 6, pp. 1551-1555, Dec, 2001.

[60] S. Agaoglu, P. Diep, M. Martini, S. Kt, M. Baday, and I. E. Araci, "Ultra-sensitive microfluidic wearable strain sensor for intraocular pressure monitoring," *Lab Chip,* vol. 18, no. 22, pp. 3471-3483, Nov 6, 2018.

[61] E. Sollier, C. Murray, P. Maoddi, and D. Di Carlo, "Rapid prototyping polymers for microfluidic devices and high pressure injections," *Lab Chip,* vol. 11, no. 22, pp. 3752-3765, Nov, 2011.

[62] H. B. An, L. Z. Chen, X. J. Liu, B. Zhao, H. Zhang, and Z. G. Wu, "Microfluidic contact lenses for unpowered, continuous and non-invasive intraocular pressure monitoring," *Sensors and Actuators a-Physical,* vol. 295, pp. 177-187, Aug, 2019.

[63] B. Maeng, H. K. Chang, and J. Park, "Photonic crystal-based smart contact lens for continuous intraocular pressure monitoring," *Lab Chip,* vol. 20, no. 10, pp. 1740-1750, May, 2020.

[64] P. J. Chen, D. C. Rodger, M. S. Humayun, and Y. C. Tai, "Unpowered spiral-tube parylene pressure sensor for intraocular pressure sensing," *Sensors and Actuators a-Physical,* vol. 127, no. 2, pp. 276-282, Mar, 2006.

[65] M. Miyashita, N. Ito, S. Ikeda, T. Murayama, K. Oguma, and J. Kimura, "Development of urine glucose meter based on micro-planer amperometric biosensor and its clinical application for self-monitoring of urine glucose," *Biosens Bioelectron,* vol. 24, no. 5, pp. 1336-40, Jan, 2009.

[66] M. X. Chu, K. Miyajima, D. Takahashi, T. Arakawa, K. Sano, S. Sawada, H. Kudo, Y. Iwasaki, K. Akiyoshi, M. Mochizuki, and K. Mitsubayashi, "Soft contact lens biosensor for in situ monitoring of tear glucose as non-invasive blood sugar assessment," *Talanta,* vol. 83, no. 3, pp. 960-965, Jan, 2011.

[67] Y. T. Liao, H. F. Yao, A. Lingley, B. Parviz, and B. P. Otis, "A 3-mu W CMOS Glucose Sensor for Wireless Contact-Lens Tear Glucose Monitoring," *Ieee Journal of Solid-State Circuits,* vol. 47, no. 1, pp. 335-344, Jan, 2012.

[68] H. Yao, C. Marcheselli, A. Afanasiev, I. Lahdesmaki, and B. A. Parviz, "A Soft Hydrogel Contact Lens with an Encapsulated Sensor for Tear Glucose Monitoring," *2012 Ieee 25th International Conference on Micro Electro Mechanical Systems (Mems)*, 2012.

[69] H. F. Yao, A. J. Shum, M. Cowan, I. Lahdesmaki, and B. A. Parviz, "A contact lens with embedded sensor for monitoring tear glucose level," *Biosensors & Bioelectronics,* vol. 26, no. 7, pp. 3290-3296, Mar, 2011.

[70] A. Afanasiev, H. Yao, C. Marcheselli, I. Lähdesmäki, and B. A. Parviz, "A synthetic eye platform for testing contact lenses with integrated electronic biosensors," *11th IEEE Conf. Nanotechnol.*, pp. 358-361, Aug, 2011.

[71] S. Halldorsson, E. Lucumi, R. Gomez-Sjoberg, and R. M. T. Fleming, "Advantages and challenges of microfluidic cell culture in polydimethylsiloxane devices," *Biosens Bioelectron,* vol. 63, pp. 218-231, Jan, 2015.

[72] S. Li, Z. Ma, Z. Cao, L. Pan, and Y. Shi, "Advanced Wearable Microfluidic Sensors for Healthcare Monitoring," *Small,* vol. 16, no. 9, pp. e1903822, Mar, 2020.

[73] R. V. Nair, and R. Vijaya, "Photonic crystal sensors: An overview," *Progress in Quantum Electronics,* vol. 34, no. 3, pp. 89-134, May, 2010.

[74] X. F. Wang, J. Engel, and C. Liu, "Liquid crystal polymer (LCP) for MEMS: processes and applications," *Journal of Micromechanics and Microengineering,* vol. 13, no. 5, pp. 628-633, Sep, 2003.

[75] N. Abdullah, A. Abu Talib, A. A. Jaafar, M. A. M. Salleh, and W. T. Chong, "The basics and issues of Thermochromic Liquid Crystal Calibrations," *Experimental Thermal and Fluid Science,* vol. 34, no. 8, pp. 1089-1121, Nov, 2010.

[76] I. Sage, "Thermochromic liquid crystals," *Liquid Crystals,* vol. 38, no. 11-12, pp. 1551-1561, 2011.

[77] R. G. Egdell, and E. Bruton, "Henry Moseley, X-ray spectroscopy and the periodic table," *Philosophical Transactions of the Royal Society A: Mathematical, Physical and Engineering Sciences,* vol. 378, no. 2180, 2020.

[78] R. Moreddu, M. Elsherif, H. Butt, D. Vigolo, and A. K. Yetisen, "Contact lenses for continuous corneal temperature monitoring," *RSC Advances,* vol. 9, no. 20, pp. 11433-11442, 2019.

[79] T. Gevers, and A. W. M. Smeulders, "Color-based object recognition," *Pattern Recognition,* vol. 32, no. 3, pp. 453-464, 1999.

[80] M. Riesenhuber, and T. Poggio, "Hierarchical models of object recognition in cortex," *Nature Neuroscience,* vol. 2, no. 11, 1999.

[81] S. Garshasbi, and M. Santamouris, "Using advanced thermochromic technologies in the built environment: Recent development and potential to decrease the energy consumption and fight urban overheating," *Solar Energy Materials and Solar Cells,* vol. 191, pp. 21-32, 2019.

[82] Y.-R. Lin, C.-C. Hung, H.-Y. Chiu, B.-H. Chang, B.-R. Li, S.-J. Cheng, J.-W. Yang, S.-F. Lin, and G.-Y. Chen, "Noninvasive Glucose Monitoring with a Contact Lens and Smartphone," *Sensors (Basel, Switzerland),* vol. 18, no. 10, pp. 3208, 2018.

[83] R. Badugu, B. H. Jeng, E. A. Reece, and J. R. Lakowicz, "Contact lens to measure individual ion concentrations in tears and applications to dry eye disease," *Analytical Biochemistry,* vol. 542, pp. 84-94, 2018.

[84] D. Dias, and J. Paulo Silva Cunha, "Wearable Health Devices-Vital Sign Monitoring, Systems and Technologies," *Sensors (Basel, Switzerland),* vol. 18, no. 8, pp. 2414, 2018.

[85] A. C. Kevat, D. V. R. Bullen, P. G. Davis, and C. O. F. Kamlin, "A systematic review of novel technology for monitoring infant and newborn heart rate," *Acta Paediatrica,* vol. 106, no. 5, pp. 710-720, 2017.

[86] G. Walker, "A review of technologies for sensing contact location on the surface of a display," *Journal of the Society for Information Display,* vol. 20, no. 8, pp. 413-440, 2012.

[87] B. Y. Won, and H. G. Park, "A Touchscreen as a Biomolecule Detection Platform," *Angewandte Chemie International Edition,* vol. 51, no. 3, pp. 748-751, 2012.

[88] B. A. Ganji, and M. Shahiri-Tabarestani, "A novel high sensitive MEMS intraocular capacitive pressure sensor," *Microsystem Technologies,* vol. 19, no. 2, pp. 187-194, 2013.

[89] M. H. Ghaed, G. Chen, R. Haque, M. Wieckowski, Y. Kim, G. Kim, Y. Lee, I. Lee, D. Fick, D. Kim, M. Seok, K. D. Wise, D. Blaauw, and D. Sylvester, "Circuits for a Cubic-Millimeter Energy-Autonomous Wireless Intraocular Pressure Monitor," *IEEE Transactions on Circuits and Systems I: Regular Papers,* vol. 60, no. 12, pp. 3152-3162, 2013.

[90] K. Ibrahim, and G. Khanna, "Optimum design of a capacitive pressure sensor," *Int. Conf. on Comp. for Sus. Glo. Dev.*, pp. 1685-1688, March, 2016.

[91] P. Chen, D. C. Rodger, S. Saati, M. S. Humayun, and Y. Tai, "Microfabricated Implantable Parylene-Based Wireless Passive Intraocular Pressure Sensors," *Journal of Microelectromechanical Systems,* vol. 17, no. 6, pp. 1342-1351, 2008.

[92] M. Ali, A. C. W. Noorakma, N. Yusof, W. N. F. Mohamad, N. Soin, and S. F. W. M. Hatta, "Optimization of MEMS intraocular capacitive pressure sensor," *IEEE Int. Conf. on Semi. Elec.*, pp. 173-176, Aug, 2016.

[93] J.-C. Chiou, Y.-C. Huang, and G.-T. Yeh, "A capacitor-based sensor and a contact lens sensing system for intraocular pressure monitoring," *Journal of Micromechanics and Microengineering,* vol. 26, no. 1, pp. 015001, 2015.

[94] J.-C. Chiou, S.-H. Hsu, Y.-C. Huang, G.-T. Yeh, W.-T. Liou, and C.-K. Kuei, "A Wirelessly Powered Smart Contact Lens with Reconfigurable Wide Range and Tunable Sensitivity Sensor Readout Circuitry," *Sensors (Basel, Switzerland),* 17, 2017.

[95] J. Chiou, S. Hsu, Y. Liao, Y. Huang, G. Yeh, C. Kuei, and K. Dai, "Toward a Wirelessly Powered On-Lens Intraocular Pressure Monitoring System," *IEEE Journal of Biomedical and Health Informatics,* vol. 20, no. 5, pp. 1216-1224, 2016.

[96] G.-Z. Chen, I.-S. Chan, L. K. K. Leung, and D. C. C. Lam, "Soft wearable contact lens sensor for continuous intraocular pressure monitoring," *Medical Engineering & Physics,* vol. 36, no. 9, pp. 1134-1139, 2014.

[97] M. Leonardi, P. Leuenberger, D. Bertrand, A. Bertsch, and P. Renaud, "First Steps toward Noninvasive Intraocular Pressure Monitoring with a Sensing Contact Lens," *Investigative Ophthalmology & Visual Science,* vol. 45, no. 9, pp. 3113-3117, 2004.

[98] M. Leonardi, P. Leuenberger, D. Bertrand, A. Bertsch, and P. Renaud, "A soft contact lens with a MEMS strain gage embedded for intraocular pressure monitoring." pp. 1043-1046 vol.2.

[99] M. Leonardi, E. M. Pitchon, A. Bertsch, P. Renaud, and A. Mermoud, "Wireless contact lens sensor for intraocular pressure monitoring: assessment on enucleated pig eyes," *Acta Ophthalmologica,* vol. 87, no. 4, pp. 433-437, 2009.

[100] S. B. Dunbar GE, Aref AA. , "The Sensimed Triggerfish contact lens sensor: efficacy, safety, and patient perspectives," *Clin Ophthalmol,* vol. 11, pp. 875-882, 2017.

[101] C. Posarelli, P. Ortenzio, A. Ferreras, M. D. Toro, A. Passani, P. Loiudice, F. Oddone, G. Casini, and M. Figus, "Twenty-Four-Hour Contact Lens Sensor Monitoring of Aqueous Humor Dynamics in Surgically or Medically Treated Glaucoma Patients," *Journal of Ophthalmology,* vol. 2019, pp. 9890831, 2019.

[102] S. M. Ittoop, J. R. SooHoo, L. K. Seibold, K. Mansouri, and M. Y. Kahook, "Systematic Review of Current Devices for 24-h Intraocular Pressure Monitoring," *Advances in Therapy,* vol. 33, no. 10, pp. 1679-1690, 2016.

[103] R. Hubanova, F. Aptel, C. Chiquet, B. Mottet, and J.-P. Romanet, "Effect of overnight wear of the Triggerfish® sensor on corneal thickness measured by Visante® anterior segment optical coherence tomography," *Acta Ophthalmologica,* vol. 92, no. 2, pp. e119-e123, 2014.

[104] I. Sánchez, V. Laukhin, A. Moya, R. Martin, F. Ussa, E. Laukhina, A. Guimera, R. Villa, C. Rovira, J. Aguiló, J. Veciana, and J. C. Pastor, "Prototype of a Nanostructured Sensing Contact Lens for Noninvasive Intraocular Pressure Monitoring," *Investigative Ophthalmology & Visual Science,* vol. 52, no. 11, pp. 8310-8315, 2011.

[105] V. Laukhin, I. Sánchez, A. Moya, E. Laukhina, R. Martin, F. Ussa, C. Rovira, A. Guimera, R. Villa, J. Aguiló, J.-C. Pastor, and J. Veciana, "Non-invasive intraocular pressure monitoring with a contact lens engineered with a nanostructured polymeric sensing film," *Sensors and Actuators A: Physical,* vol. 170, no. 1, pp. 36-43, 2011.

[106] R. Durà, F. Mathieu, L. Nicu, F. Pérez-Murano, and F. Serra-Graells, "A 0.3-mW/Ch 1.25 V piezo-resistance digital ROIC for liquid-dispensing MEMS," *Trans. Cir. Sys. Part I,* vol. 56, no. 5, pp. 957–965, 2009.

[107] N. Thomas, I. Lähdesmäki, and B. A. Parviz, "A contact lens with an integrated lactate sensor," *Sensors and Actuators B: Chemical,* vol. 162, no. 1, pp. 128-134, 2012.

[108] D. H. Keum, S.-K. Kim, J. Koo, G.-H. Lee, C. Jeon, J. W. Mok, B. H. Mun, K. J. Lee, E. Kamrani, C.-K. Joo, S. Shin, J.-Y. Sim, D. Myung, S. H. Yun, Z. Bao, and S. K. Hahn, "Wireless smart contact lens for diabetic diagnosis and therapy," *Science Advances,* vol. 6, no. 17, pp. eaba3252, 2020.

[109] M. Donora, A. Vásquez Quintero, H. De Smet, and I. Underwood, "Spatiotemporal electrochemical sensing in a smart contact lens," *Sensors and Actuators B: Chemical,* vol. 303, pp. 127203, 2020.

[110] P. G. Boswell, and P. Bühlmann, "Fluorous Bulk Membranes for Potentiometric Sensors with Wide Selectivity Ranges: Observation of Exceptionally Strong Ion Pair Formation," *Journal of the American Chemical Society,* vol. 127, no. 25, pp. 8958-8959, 2005.

[111] D. R. Nasreldin M, Ramuz M, Lahuec C, Djenizian T, de Bougrenet de la Tocnaye J-L, " Flexible Micro-Battery for Powering Smart Contact Lens," *Sensors,* vol. 19, no. 9, May, 2019.

[112] J. Pandey, Y. Liao, A. Lingley, R. Mirjalili, B. Parviz, and B. P. Otis, "A Fully Integrated RF-Powered Contact Lens With a Single Element Display," *IEEE Transactions on Biomedical Circuits and Systems,* vol. 4, no. 6, pp. 454-461, 2010.

[113] D. M. Pozar, *Microwave Engineering*, Hoboken: Wiley, 2012.

[114] W. L. Stutzman, and G. A. Thiele, *Antenna Theory and Design*: Wiley, 2012.

[115] L. Y. Chen, B. Milligan, T. Qu, L. Jeevananthan, G. Shaker, and S. Safavi-Naeini, "Cellular Wireless Energy Harvesting for Smart Contact Lens Applications," *Ieee Antennas and Propagation Magazine,* vol. 60, no. 5, pp. 108-124, Oct, 2018.

[116] T. Takamatsu, Y. Sijie, F. Shujie, L. Xiaohan, and T. Miyake, "Multifunctional High-Power Sources for Smart Contact Lenses," *Advanced Functional Materials,* vol. 30, no. 29, pp. 1906225, 2020.

[117] A. R. Lingley, M. Ali, Y. Liao, R. Mirjalili, M. Klonner, M. Sopanen, S. Suihkonen, T. Shen, B. P. Otis, H. Lipsanen, and B. A. Parviz, "A single-pixel wireless contact lens display," *Journal of Micromechanics and Microengineering,* vol. 21, no. 12, pp. 125014, 2011.

[118] J. Chiou, S. Hsu, C. Kuei, and T. Wu, "An addressable UHF EPCGlobal Class1 Gen2 Sensor IC for wireless IOP monitoring on contact lens," *Conf. on VLSI Des. Autom. & Test.*, pp. 1-4, April, 2015.

[119] C. Jeon, J. Koo, K. Lee, M. Lee, S. Kim, S. Shin, S. K. Hahn, and J. Sim, "A Smart Contact Lens Controller IC Supporting Dual-Mode Telemetry With Wireless-Powered Backscattering LSK and EM-Radiated RF Transmission Using a Single-Loop Antenna," *IEEE Journal of Solid-State Circuits,* vol. 55, no. 4, pp. 856-867, 2020, 2020.

[120] H. W. Cheng, B. M. Jeng, C. Y. Chen, H. Y. Huang, J. C. Chiou, and C. H. Luo, "The rectenna design on contact lens for wireless powering of the active intraocular pressure monitoring system," *35th Annual Int. Conf. IEEE Eng. in Med. & Biol. Soc.*, pp. 3447-3450, Jul, 2013.

[121] L. Chen, G. Shaker, and S. Safavi-Naeini, "Energy harvesting system integrated on wearable contact lens," *IEEE Int. Symp. on Antennas. Propag. & USNC/URSI Nat. Radio Sci. Meeting,* pp. 358-359, June, 2015.

[122] J. C. Lin, "A new IEEE standard for safety levels with respect to human exposure to radio-frequency radiation," *IEEE Antennas and Propagation Magazine,* vol. 48, no. 1, pp. 157-159, 2006.

[123] V. G. Motti, and K. Caine, "Human Factors Considerations in the Design of Wearable Devices," *Proceedings of the Human Factors and Ergonomics Society Annual Meeting,* vol. 58, no. 1, pp. 1820-1824, 2014.

[124] L. Y. Chen, B. C. K. Tee, A. L. Chortos, G. Schwartz, V. Tse, D. J. Lipomi, H. S. P. Wong, M. V. McConnell, and Z. Bao, "Continuous wireless pressure monitoring and mapping with ultra-small passive sensors for health monitoring and critical care," *Nature Communications,* vol. 5, no. 1, pp. 5028, 2014.

[125] J. Kaiser, "The Archimedean two-wire spiral antenna," *IRE Transactions on Antennas and Propagation,* vol. 8, no. 3, pp. 312-323, 1960.

[126] J. C. G. Matthews, B. Pirollo, A. Tyler, and G. Pettitt, "Body wearable antennas for UHF/VHF," *Loughborough Antennas & Propag. Conf.*, pp. 357-360, Mar, 2008.

[127] J. Zhong, A. Kiourti, T. Sebastian, Y. Bayram, and J. L. Volakis, "Conformal Load-Bearing Spiral Antenna on Conductive Textile Threads," *IEEE Antennas and Wireless Propagation Letters,* vol. 16, pp. 230-233, 2017.

[128] S. H. Lee, J. Lee, Y. J. Yoon, S. Park, C. Cheon, K. Kim, and S. Nam, "A Wideband Spiral Antenna for Ingestible Capsule Endoscope Systems: Experimental Results in a Human Phantom and a Pig," *IEEE Transactions on Biomedical Engineering,* vol. 58, no. 6, pp. 1734-1741, 2011.

[129] M. Yuan, R. Das, R. Ghannam, Y. Wang, J. Reboud, R. Fromme, F. Moradi, and H. Heidari, "Electronic Contact Lens: A Platform for Wireless Health Monitoring Applications," *Advanced Intelligent Systems,* vol. 2, no. 4, pp. 1900190, 2020.

[130] J. C. Lin, Y. Zhao, P. Chen, and Y. Tai, "High quality factor parylene-based intraocular pressure sensor," *7th IEEE Int. Conf. on Nano/Micro Engineered & Mol. Syst.*, pp. 137-140, March, 2012.

[131] G.-Z. Chen, I.-S. Chan, and D. C. C. Lam, "Capacitive contact lens sensor for continuous non-invasive intraocular pressure monitoring," *Sensors and Actuators A: Physical,* vol. 203, pp. 112-118, 2013.

[132] J. Kim, M. Kim, M.-S. Lee, K. Kim, S. Ji, Y.-T. Kim, J. Park, K. Na, K.-H. Bae, H. Kyun Kim, F. Bien, C. Young Lee, and J.-U. Park, "Wearable smart sensor systems integrated on soft contact lenses for wireless ocular diagnostics," *Nature Communications,* vol. 8, no. 1, pp. 14997, 2017.

[133] H. Yasuda, "Biocompatibility of Nanofilm-Encapsulated Silicone and Silicone-Hydrogel Contact Lenses," *Macromolecular Bioscience,* vol. 6, no. 2, pp. 121-138, 2006.

[134] C. S. A. Musgrave, and F. Fang, "Contact Lens Materials: A Materials Science Perspective," *Materials (Basel, Switzerland),* vol. 12, no. 2, pp. 261, 2019.

[135] M. Holzinger, A. Le Goff, and S. Cosnier, "Nanomaterials for biosensing applications: a review," *Frontiers in Chemistry,* vol. 2, no. 63, 2014.

[136] A. Shahini, M. Hajizadegan, M. Sakhdari, M. M. C. Cheng, P. Chen, and H. H. Huang, "Self-powered and transparent all-graphene biosensor," *IEEE Sensors Conf.*, pp. 1-3, Nov, 2016.

[137] M. J. Large, M. Cann, S. P. Ogilvie, A. A. K. King, I. Jurewicz, and A. B. Dalton, "Finite-size scaling in silver nanowire films: design considerations for practical devices," *Nanoscale,* vol. 8, no. 28, pp. 13701-13707, 2016.

[138] K. S. Kim, Y. Zhao, H. Jang, S. Y. Lee, J. M. Kim, K. S. Kim, J.-H. Ahn, P. Kim, J.-Y. Choi, and B. H. Hong, "Large-scale pattern growth of graphene films for stretchable transparent electrodes," *Nature,* vol. 457, no. 7230, pp. 706-710, 2009.

[139] X. Li, W. Cai, J. An, S. Kim, J. Nah, D. Yang, R. Piner, A. Velamakanni, I. Jung, E. Tutuc, S. K. Banerjee, L. Colombo, and R. S. Ruoff, "Large-Area Synthesis of High-Quality and Uniform Graphene Films on Copper Foils," *Science,* vol. 324, no. 5932, pp. 1312, 2009.

[140] J.-U. Park, S. Nam, M.-S. Lee, and C. M. Lieber, "Synthesis of monolithic graphene–graphite integrated electronics," *Nature Materials,* vol. 11, no. 2, pp. 120-125, 2012.

[141] R. R. Nair, P. Blake, A. N. Grigorenko, K. S. Novoselov, T. J. Booth, T. Stauber, N. M. R. Peres, and A. K. Geim, "Fine Structure Constant Defines Visual Transparency of Graphene," *Science,* vol. 320, no. 5881, pp. 1308, 2008.

[142] C. M. Portela, A. Vidyasagar, S. Krödel, T. Weissenbach, D. W. Yee, J. R. Greer, and D. M. Kochmann, "Extreme mechanical resilience of self-assembled nanolabyrinthine materials," *Proceedings of the National Academy of Sciences,* vol. 117, no. 11, pp. 5686, 2020.

[143] J. Park, J. Kim, S.-Y. Kim, W. H. Cheong, J. Jang, Y.-G. Park, K. Na, Y.-T. Kim, J. H. Heo, C. Y. Lee, J. H. Lee, F. Bien, and J.-U. Park, "Soft, smart contact lenses with integrations of wireless circuits, glucose sensors, and displays," *Science Advances,* vol. 4, no. 1, pp. eaap9841, 2018.

[144] Y. Shi, L. He, Q. Deng, Q. Liu, L. Li, W. Wang, Z. Xin, and R. Liu, "Synthesis and Applications of Silver Nanowires for Transparent Conductive Films," *Micromachines,* vol. 10, no. 5, pp. 330, 2019.

[145] J. Park, D. B. Ahn, J. Kim, E. Cha, B.-S. Bae, S.-Y. Lee, and J.-U. Park, "Printing of wirelessly rechargeable solid-state supercapacitors for soft, smart contact lenses with continuous operations," *Science Advances,* vol. 5, no. 12, pp. eaay0764, 2019.
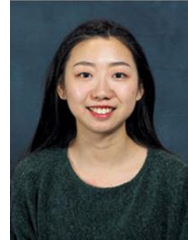
Mengyao Yuan received her B.Eng. Degree in Electrical and Electronics Engineering, University of Electronic Science and Technology of China, 2018 and received an M.Sc. degree in Electrical & Electronics Engineering, University, of Glasgow, 2019. She is currently a PhD student in Microelectronics Laboratory (meLAB) at University of Glasgow and her research interest is wireless power transfer on wearable electronics.

Rupam Das received the M.Sc. and Ph.D. degrees in Biomedical Engineering from the University of Ulsan, Ulsan, South Korea, in 2013 and 2017, respectively. He was a Post-Doctoral Associate of Electrical Engineering with the University of Ulsan before joining to the meLAB. He has been recently awarded the prestigious Marie Curie Fellowship to work on wireless neural implants. His current research interests include wireless power transfer, microelectronics, MRI safety, metamaterials, implantable devices and antennas.

Eve McGlynn received her M.Eng. degree in electronic and electrical engineering from the University of Glasgow, U.K. in 2019, with a focus on antenna design. She is currently pursuing her Ph.D. as part of the Microelectronics Lab at the University of Glasgow. Her research is centred around the design and fabrication of implantable brain devices, using nanofabrication techniques.

Rami Ghannam (BEng, DIC, MSc, PhD, MIET, SMIEEE) is a lecturer (Assistant Professor) in Electronic and Nanoscale Engineering. Following his PhD. from Cambridge University in 2007, Dr. Ghannam spent the past ten years in the field of photovoltaics. He has held previous appointments at Nortel Networks and IBM Research GmbH. He received his B.Eng. degree from King's College, as well as his DIC and M.Sc. degrees from Imperial College London. Dr. Ghannam is currently investigating the use of energy harvesters for wearable and implantable electronic devices. He is a member of the IET and a Senior Member of the IEEE.

Qammer Abassi (SM'16) received the B.Sc. and M.Sc. degrees in electronics and telecommunication engineering from the University of Engineering and Technology (UET), Lahore, Pakistan, and the Ph.D. degree in electronic and electrical engineering from the Queen Mary University of London (QMUL), 2012. He is currently a Senior Lecturer (Associate Professor) with the James Watt School of Engineering, University of Glasgow, U.K., deputy head for Communication Sensing and Imaging group and research investigator with Scotland 5G Center. He has contributed to over 300 leading international technical journal and peer reviewed conference papers, and eight books. He received several recognitions for his research, which include appearance on BBC, STV, dawnnews, local and international newspapers, cover of MDPI journal, most downloaded

13

articles, U.K. exceptional talent endorsement by Royal Academy of Engineering, National Talent Pool Award by Pakistan, International Young Scientist Award by NSFC China, URSI Young Scientist Award, National Interest Waiver by USA, four best paper awards, and best representative image of an outcome by QNRF. He is an Associate Editor for the IEEE JOURNAL OF ELECTROMAGNETICS, RF AND MICROWAVES IN MEDICINE AND BIOLOGY, the IEEE SENSORS JOURNAL, IEEE OPEN ACCESS ANTENNA AND PROPAGATION, IEEE ACCESS and acted as a guest editor for numerous special issues in top notch journals

Hadi Heidari (M'15–SM'17) is an Associate Professor (Senior Lecturer) in the James Watt School of Engineering at the University of Glasgow, UK. He is leading the Microelectronics Laboratory (meLAB) and his research includes developing microelectronics for wearable and implantable devices. He is a member of the IEEE Circuits and Systems Society Board of Governors (2018–2020), IEEE Sensors Council Member-at-Large (2020-2021), senior member of IEEE and Fellow of Higher Education Academy (FHEA). He is the General Chair of the 27th IEEE ICECS 2020, and serves on the organizing committee of several international conferences.